Int. J. Electrochem. Sci., 8 **(2013)** 8740 - 8751

International Journal of
ELECTROCHEMICAL
SCIENCE
www.electrochemsci.org

Synthesis, Characterization and Electrochemical Performance of Manganese Dioxide in a Quaternary Microemulsion: the Role of the Co-surfactant and Water

Baohua Li[1,*], *Guangyao Gao*[1,2], *Dengyun Zhai*[1,2], *Chunguang Wei*[1,2], *Yanbing He*[1], *Hongda Du*[1] *and Feiyu Kang*[1,2]

[1] Engineering Laboratory for Functionalized Carbon Materials and Key Laboratory of Thermal Management Engineering and Materials, Graduate School at Shenzhen, Tsinghua University, Shenzhen, Guangdong Province, 518055, P. R. China.
[2] Department of Materials Science & Engineering, Tsinghua University, Beijing, 100084, P. R. China.
[*]E-mail: libh@mail.sz.tsinghua.edu.cn

Received: 30 March 2013 / *Accepted:* 29 April 2013 / *Published:* 1 June 2013

Manganese dioxide nanoparticles were synthesized in a quaternary microemulsion using surfactant hexadecyl-trimethylammonium bromide. The structure and morphology of the as-prepared manganese dioxide powders were characterized by means of powder X-ray diffraction, scanning electron microscopy and transmission electron microscopy. The average size of nanoparticles, as well as the crystalline structure of manganese dioxide, can be controlled by the content of co-surfactant n-pentanol and water. The particle size decreased with adding the amount of n-pentanol or reducing water, and simultaneously manganese dioxide nanosheets were generated. Their electrochemical properties were investigated using cyclic voltammetry in 0.1 M Na_2SO_4 electrolyte. The specific capacitance of the as-prepared manganese dioxide powder with the surface area of 231.5 m^2 g^{-1} was 140.5 F g^{-1} at scanning rate of 2 mV s^{-1}.

Keywords: Manganese dioxide, supercapacitor, microemulsion, co-surfactant.

1. INTRODUCTION

In recent years, supercapacitors have attracted more and more attentions because they can offer higher powder density and have the excellent cyclicity [1]. Based on the charge-storage mechanism, supercapacitors are divided into two types: electrical double-layer capacitors (EDLCs) and Faradic pseudocapacitors. EDLCs are based on the double-layer effect of carbon materials with high surface area and Faradic pseudocapacitors are caused by a faradic charge exchange reaction. Some noble or transition metal oxides show pseudo-capacitive behavior. For example, amorphous hydrous ruthenium dioxide (RuO_2) has a high specific capacitance (760 F g^{-1}) in H_2SO_4 solution [2]. Compared to RuO_2

with high cost, Manganese dioxide (MnO_2) is inexpensive, environmentally friendly, and abundant in raw materials [3]. Since Lee and Good-enough found its ideal capacitive behavior, MnO_2 has attracted more interest due to its possible application in future.

Various methods have been reported to synthesize MnO_2, including thermal decomposition [4], template method [5], hydrothermal reaction [6], and microemulsion methods [7-9], etc. Microemulsion-based synthesis has been proved to be a useful method to synthesize a variety of nanostructured nanoparticles. This method enables researchers to synthesize nanomaterials with varied size and shape (such as nanosphere, nanotube, nanowire, etc) by altering various components involved in the formation of microemulsion [10-12]. "Water-in-oil" microemulsion is composed of aqueous nano droplets and continuous oil medium, which are stabilized by surfactant and co-surfactant located at the water/oil interface. Devarj and Munichandraiah [8] synthesized MnO_2 particles in the spherical/hexagonal shape with about 50 nm size by microemulsion method. Xu *et al*. [9] reported a self-reacting microemulsion method by which MnO_2 nanosphere with the diameter of 4 nm was synthesized. However, there are few reports concerning the changes of the size and crystalline structure of MnO_2 by altering the content of co-surfactant and water in the microemulsion system. The nano water droplets can be seen as nanoreactors in a microemulsion system, and the size or the stability of nanoparticles could be adjusted during the reaction [13-17] by altering the content of the co-surfactant and the water.

In this paper, we chose n-hexane (NH) as the oil phase, hexadecyl-trimethylammonium bromide (CTAB) as the surfactant, n-pentanol (NP) as the co-surfactant. As far as the quaternary microemulsion is concerned, there are three factors that determine the formation of microemulsion: the molar ratio between water and surfactant (W_0), that molar ratio between co-surfactant and surfactant (P_0), and the molar concentration of the surfactant (S). The aqueous phase of the reverse micelles plays an important role in determining the size of the final products [18]. Nano water droplets surrounding the reactants, are the places where the reaction occurs, and the particle size is determinate by the size of droplets which is a function of W_0. Pileni's group [11] pioneered the studies about the controlling of nanoparticles' size and shape by varying W_0, and showed that the size of copper nanoparticles increases with increasing water content. The role of a co-surfactant is to lower the interfacial tension between the oil and water for the spontaneous formation of surfactant aggregates [14]. Curri *et al* reported that Cadmium sulfide (CdS) nanoparticles were synthesized in a quaternary CTAB/NP/NH/water microemulsion with NP as the co-surfactant, and the average size of the CdS nanoparticles was also controlled by the NP content [19]. Therefore, here we studied intensively the role of the co-surfactant NP and water as potentially useful parameters in controlling the size and crystalline structure of MnO_2.

2. EXPERIMENTAL DETAILS

2.1 Preparation of MnO_2 with different P_0

The MnO_2 powders were synthesized by a microemulsion route, as shown in Fig.1. The quaternary microemulsion system was composed of CTAB, water, NP, and NH. The oil phase was

NH, and CTAB was chosen as the surfactant and NP as the co-surfactant. The concentration of CTAB in oil phase was 0.1M. W_0 was 10, and P_0 was 5, 10, 15. Only when the value of W_0 is larger than or equal to 5, CTAB could dissolve in water and the water-in-oil system could be formed [20]. Therefore, 4.5 ml water was first added to form a water-in-oil solution. Denoted the two water-in-oil systems as A and B, added 4.5 ml water and 4.5 ml of 0.2 M $KMnO_4$ solution into system A, and 4.5 ml water and 4.5ml of 0.3 M $Mn(C_2H_3O_2)_2$ solution into B, to form nano water droplets containing reactants. Then two systems were mixed and stirred for 1 h, and the MnO_2 powder suspension was formed. After filtered with deionized water and dried for 24 h at 85 ^oC, the samples were obtained. The as-prepared powder was denoted as MnO_2-P_0-X where X represents the value of P_0.

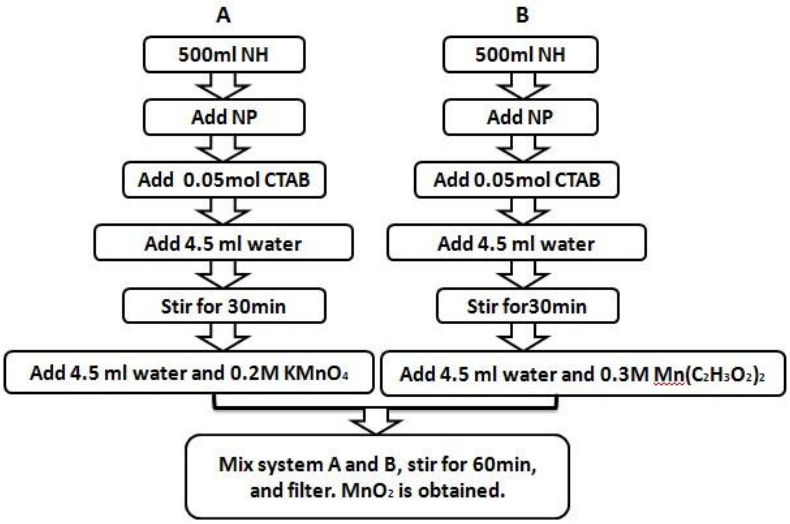

Figure 1. Process procedure for preparing MnO_2 using a microemulsion route.

2.2 Preparation of MnO_2 with different W_0

The synthesis route was the same as the above. The concentration of CTAB in oil phase was 0.1 M. Among the above all of as-prepared MnO_2-P_0-X powders, the electrochemical performance of sample MnO_2-P_0-10 is the best and thus P_0 value was fixed at 10, and W_0 was set as 10, 20, 30. In the same way, the MnO_2 powders with different W_0 were obtained, and the as-prepared powder was denoted as MnO_2-W_0-Y where Y represents the value of W_0. Because W_0 was set as 10 when preparing sample MnO_2-P_0-10, MnO_2-P_0-10 and MnO_2-W_0-10 were the same, then added samples MnO_2-W_0-20, 30.

2.3 Characterization

Powder X-ray diffraction (XRD) patterns of the samples were obtained by using a TW3040/60 diffractometer (Tanalygical Company, Holland) in which Cu-Kα (λ*=0.154 nm*) was used as the radiation source. The morphologies were examined by Hitachi S-4800 scanning electron microscopy

(SEM) and JEM-2100F transmission electron microscopy (TEM). The surface area and the pore size distribution were determined by N_2 adsorption at 77 K with an automated adsorption apparatus (Micromeritics ASAP 2020). Based on the Brunauer-Emmett-Tellr (BET) equation, the surface area was calculated. The pore size distribution was obtained by the BJH method [21] from the desorption isotherm.

2.4 Electrochemical measurement

The electrode was prepared by mixing 70 wt.% of MnO_2 powder with 20 wt.% acetylene black and 10 wt.% polytetrafluoroethylene (PTFE). The detailed procedure was as follows: 35 mg of MnO_2 powder and 10 mg of acetylene black were first mixed and dispersed in ethanol by sonication for 30 min. Then the ink was dried at 80 ^oC for 12 h and 100 mg of PTFE aqueous solution (5 wt.%) was added. After being dried at 80 ^oC, a few drops of 1-methy-2-pyrrolidinone (NMP) were added to get the syrup. The syrup was rolled into thick film. The film was cut into the 1cm × 1cm pieces of about 3 mg, and then hot-pressed at 80 ^oC under 40 Mpa onto the titanium foil as the collector.

Electrochemical tests were performed with the battery system VMP3 (Bio-Logic Corp., France). A piece of platinum gauze and a saturated calomel electrode (SCE) were assembled as the counter and reference electrode. 0.1 M Na_2SO_4 solution was used as the electrolyte.

3. RESULTS AND DISCUSSION

3.1 Characteristics of samples MnO_2 with different P_0 or W_0

Fig.2 shows the XRD patterns of samples MnO_2-P_0-5, 10, 15 when other parameters W_0 and S of microemulsion system are the constant. The presence of a few broad peaks is related to the poor crystallinity and nanoscale nanoparticles. The profiles of a few broad peaks around $2\theta=37.1^o$ and 65.6^o seem to be consistent with the peaks of γ-MnO_2 (JCPDS NO.14-0644). The peak around $2\theta=21^o$ shows the existence of γ-MnO_2 when P_0=5, and then disappears when P_0=10. By adding more NP, the appearance of a broad peak around $2\theta=12.2^o$ shows the existence of Birnessite-type MnO_2 (JCPDS NO.18-0802).

Among the above all of as-prepared MnO_2-P_0-X powders, the electrochemical performance of sample MnO_2-P_0-10 is the best and P_0 value was fixed at 10. Actually, MnO_2-P_0-10 and MnO_2-W_0-10 are the same. Fig.3 shows the XRD patterns of samples MnO_2-W_0-10, 20, 30. As discussed above, When W_0=10, 20, 30, a few broad peaks around $2\theta=37.1^o$ and 65.6^o are the same, the profile of these peaks seems to be consistent with the peaks of γ-MnO_2. By adding more water, the appearance of a broad peak around $2\theta=12.2^o$ shows the existence of Birnessite-type MnO_2.

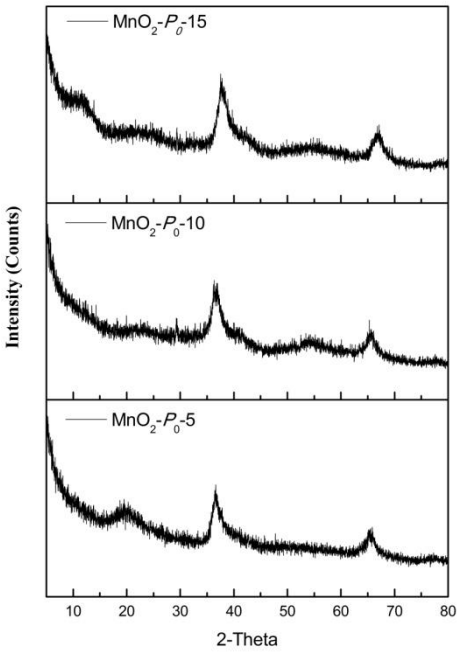

Figure 2. XRD patterns of samples MnO_2-P_0- 5, 10, 15 prepared with different P_0 when other parameters W_0 and S of microemulsion systems are the constant.

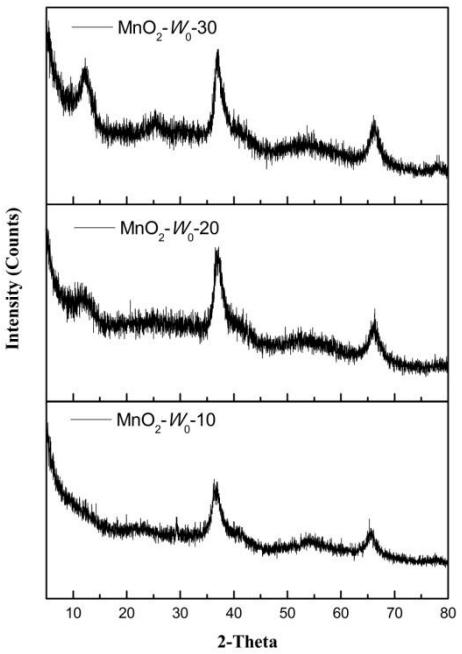

Figure 3. XRD patterns of samples MnO_2-W_0-10, 20, 30 with different W_0 when other parameters P_0 and S of microemulsion systems are the constant, P_0=10.

As discussed above, it can be concluded that the crystalline structure of MnO_2 can be controlled by changing the content of co-surfactant NP and water. With increasing the content of NP or

water, Birnessite-type MnO_2 is generated gradually among the as-prepared γ-MnO_2, which can be proved by the appearance of a broad peak around $2\theta=12.2^{o}$.

The morphology of samples MnO_2-P_0-5, 10, 15 and MnO_2-W_0-10, 20, 30 is shown as the SEM images in Fig.4, and MnO_2-P_0-15 and MnO_2-W_0-20, 30 TEM images are shown in Fig.5. It shows that MnO_2-P_0-5, 10 spherical nanoparticles agglomerate together, and MnO_2-P_0-15 has mainly spherical nanoparticles besides MnO_2 nanosheets observed by TEM image in Fig.5 (a). It can be seen that the size of spherical MnO_2 nanoparticles decreases significantly by adding more NP, because the interfacial tension between NH and water decreases gradually, the higher fluidity of the interfacial film and higher mean curvature of radius in turn make the intermicellar exchange rate higher, which implies the higher consumption of reactants at the nucleation stage, thus reduces the effective concentration for further growth, and results in smaller MnO_2 nanoparticles.

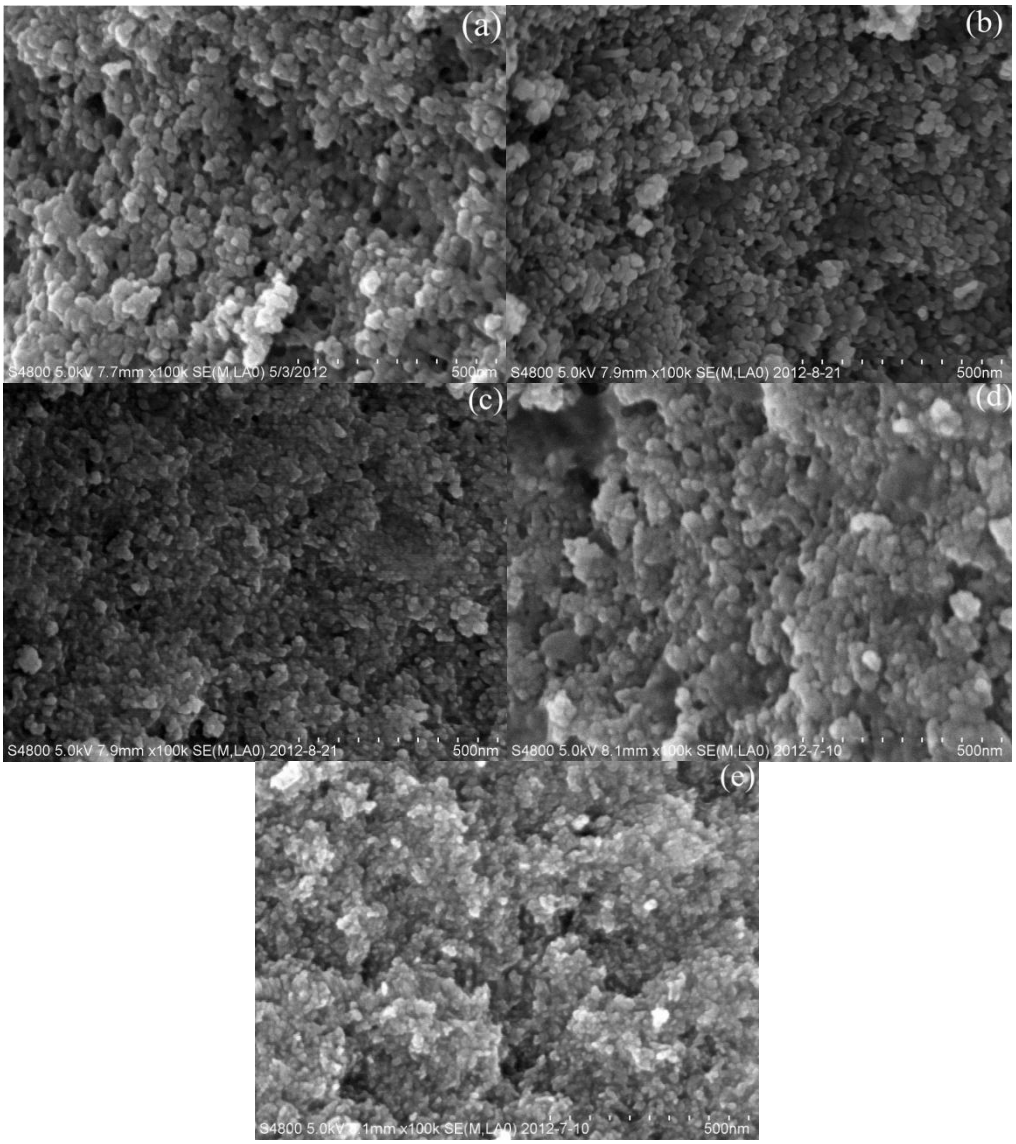

Figure 4. The morphology of samples MnO_2-P_0-5, 10, 15 (a-c), MnO_2-W_0-20, 30 (d-e), MnO_2-P_0-10 and MnO_2-W_0-10 are the same (b).

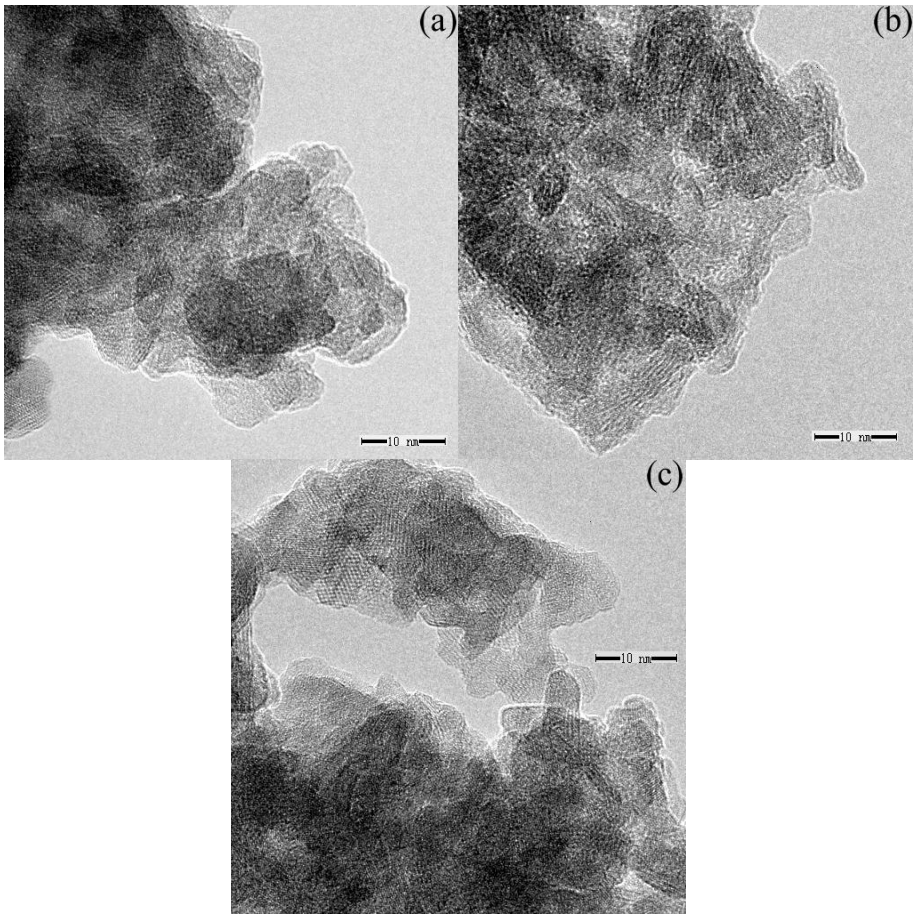

Figure 5. TEM images of samples MnO_2-P_0-15 and MnO_2-W_0-20, 30, MnO_2 nanosheets were observed in these three samples.

MnO_2-P_0-10 or MnO_2-W_0-10 is shown in Fig.4 (b), and MnO_2-W_0-20, 30 have mainly spherical nanoparticles besides MnO_2 nanosheets observed by TEM images in Fig.5 (b-c). It can be seen that the size of the spherical MnO_2 nanoparticles increases by adding more water in the system. Due to the increasing of the water content, the number of nano water droplets in the unit volume increases, greatly promoting the possibilities of collision between droplets and the exchange rate of the reactants, which implies more rapid nucleation and growth, and finally results in the larger MnO_2 nanoparticles.

Some researchers synthesized MnO_2 by microemulsion-based methods using different surfactants [8, 9, 22, 23], the results show that the size, shape and crystalline structure of MnO_2 could be changed by using different surfactants. However, the effect of co-surfactant or water on MnO_2 in a quaternary microemulsion has not been studied. In this work, we investigated this issue initially, and pointed out that the average size and the crystalline structure of MnO_2 could be controlled by altering the content of the co-surfactant NP and water as discussed above. It can be concluded that the particle size decreases when adding the amount of NP or reducing water, and MnO_2 nanosheets are generated simultaneously.

The nitrogen adsorption/desorption isotherms and the pore size distributions of samples MnO_2-P_0-5, 10, 15 are shown in Fig.6 and Fig.7, respectively. It shows that samples MnO_2-P_0-5, 10, 15 are typically mesoporous materials with different pore size distributions piled up by the nano powders,

respectively. The specific surface area of MnO_2-P_0-5 is 84.9 m^2 g^{-1}, and MnO_2-P_0-10 has a higher specific surface area of 231.5 m^2 g^{-1}, because the average size of MnO_2 nanoparticles is smaller and the spherical nanoparticles agglomerate together more easily, resulting that mesopores could be piled up by the nanoparticles (Fig.7). The specific surface area of MnO_2-P_0-15 decreases to 21.6 m^2 g^{-1} probably because MnO_2 nanosheets are generated, which may lead to the smaller surface area.

The nitrogen adsorption/desorption isotherms and the pore size distributions of samples MnO_2-W_0-10, 20, 30 are shown in Fig.8 and Fig.9, respectively. As is mentioned above, when P_0=10 and W_0=10, the as-prepared MnO_2 is typically a mesoporous material with the specific surface area of 231.5 m^2 g^{-1}. MnO_2-W_0-20, 30 are mesoporous materials with the specific surface area of 15.3, 14.5 m^2 g^{-1} probably because MnO_2 nanosheets generated have smaller surface area.

The nanoparticles size and the crystalline structure of MnO_2 which can be controlled by the content of co-surfactant NP and water, both have an influence on the pore size distributions of MnO_2 samples, which is not studied elsewhere. When P_0=10 and W_0=10, the as-prepared MnO_2 has the highest specific surface area.

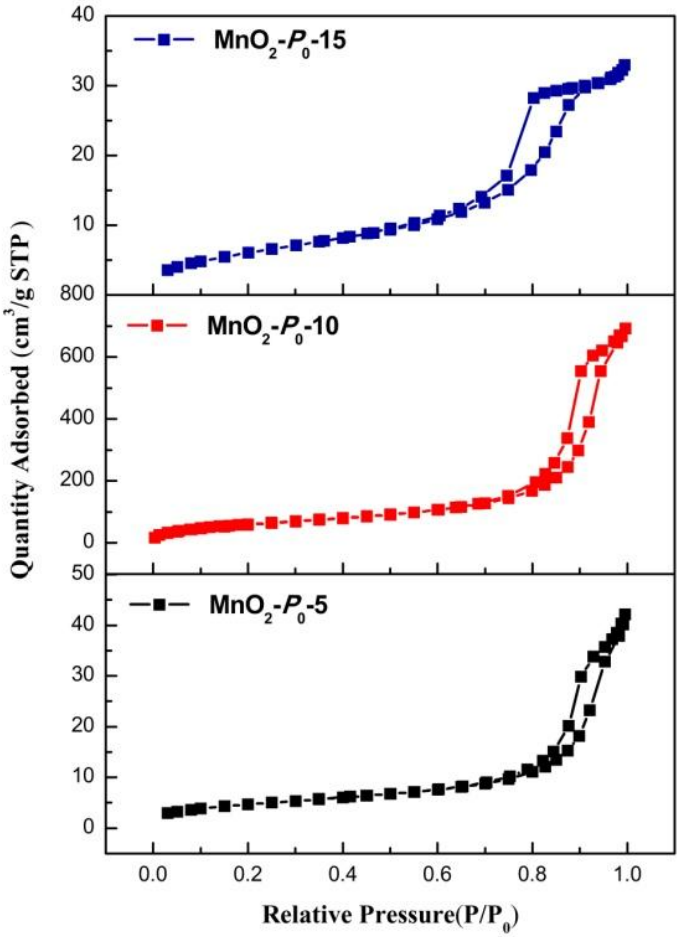

Figure 6. Nitrogen adsorption/desorption isotherms at 77K for samples MnO_2-P_0-5, 10, 15.

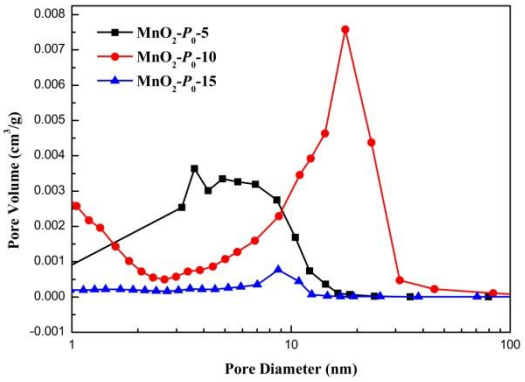

Figure 7. The pore size distribution of samples MnO_2-P_0- 5, 10, 15 calculated by BJH method.

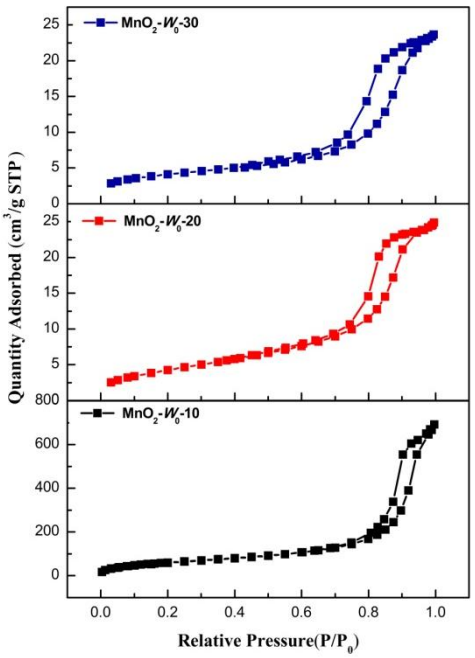

Figure 8. Nitrogen adsorption/desorption isotherms at 77K for MnO_2-W_0-10, 20, 30.

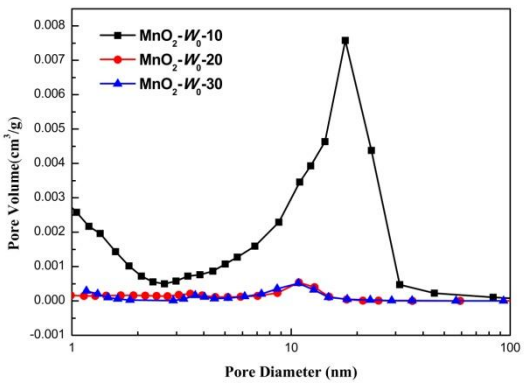

Figure 9. The pore size distribution of samples MnO_2-W_0-10, 20, 30 calculated by BJH method.

3.2 Electrochemical properties of samples MnO_2 with different P_0 or W_0

Typical cyclic voltammetry (CV) measurements were conducted for as-prepared samples in 0.1 M Na_2SO_4 solution. The potential range was 0-0.8 V versus SCE, the measurements were taken at different scanning rates from 2 to 50 mV s^{-1}. The average specific capacitance (SC) was calculated by the equation.

$$C=Q/(\Delta E\times m) \qquad (1)$$

Where C is the specific capacitance, Q is the half charge obtained after integrating the voltammogram, m is the total mess of MnO_2 material in the electrode, and ΔE is the potential window.

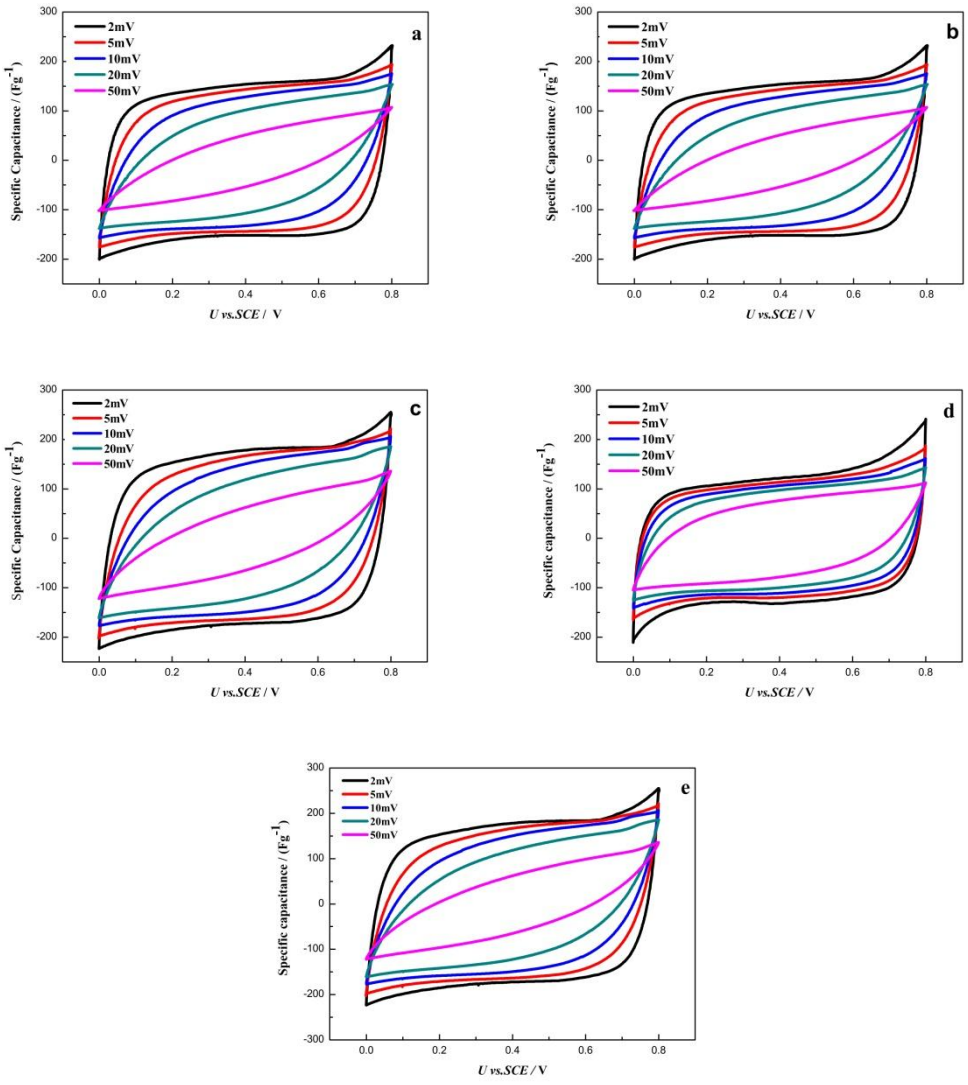

Figure 10. Cyclic voltammograms at different scanning rates in 0.1 M Na_2SO_4 electrolyte, MnO_2-P_0-5, 10, 15 (a-c), MnO_2-W_0-20, 30 (d-e), MnO_2-P_0-10 and MnO_2-W_0-10 are the same (b).

The CV curves of MnO_2 samples at different scanning rates of 2-50 mV s^{-1} are shown in Fig. 10. All the curves at the scanning rate of 2 mV s^{-1} are relatively rectangular, and the current response

to the voltage reversal exhibits near mirror-image, indicating a reversible reaction and ideal capacitive behavior. According to Eq. (1), the SC of MnO_2-P_0-5, 10, 15 calculated from CV of 2 mV s^{-1} is 117.0, 140.5 and 125.3 F g^{-1}, respectively. And the SC of MnO_2-W_0-20, 30 calculated from CV of 2 mV s^{-1} is 120.8 and 105.2 F g^{-1}, respectively. When the scanning rate increases from 2 to 50 mV s^{-1}, CV curves of MnO_2-P_0-5, 15 became distorted more dramatically than MnO_2-P_0-10 as shown in Figs.10 and 11, and MnO_2-P_0-10 has a better electrochemical performance. At the scanning rate 50 mV s^{-1}, CV curves of MnO_2-W_0-10 became distorted more dramatically than MnO_2-W_0-20, 30, the SC decreases drastically from 140.5 to 41.3 F g^{-1}.

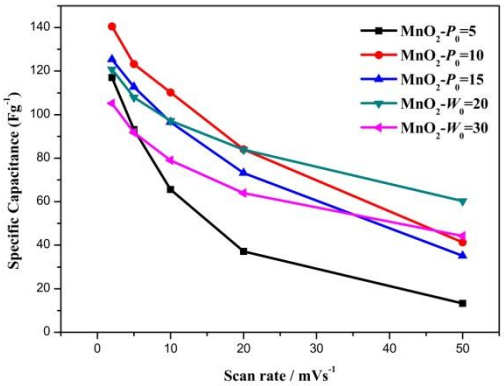

Figure 11. Dependence of the specific capacitance on the scanning rate for MnO_2-P_0-5, 10, 15, MnO_2-W_0-20, 30, and MnO_2-P_0-10 and MnO_2-W_0-10 are the same.

Compared with the previous work [8, 9, 22, 23], the two parameters in the microemulsion system were optimized in the present work: the content of the co-surfactant NP and water, and the relationship between the microstructure and the electrochemical property of MnO_2 has been studied intensively. When P_0=10 and W_0=10, the as-prepared γ-MnO_2 with the surface area of 231.5 m^2 g^{-1} had excellent electrochemical performance.

4. CONCLUSIONS

In a quaternary microemulsion composed of CTAB, water, NP, and NH, the average size of MnO_2 nanoparticles could be controlled by both the content of NP and water, and the crystalline structure also changed simultaneously. The average size of the spherical MnO_2 nanoparticles decreased due to the increasing of NP content and increased accordingly to the increasing of water content. Meanwhile, MnO_2 nanosheets were generated gradually by adding more NP or water. The specific capacitance of the as-prepared MnO_2-P_0-10 was up to 140.5 F g^{-1} at scanning rate of 2 mV s^{-1}, but its poor conductivity lead to the capacitance's decay at high scanning rate. Therefore, the further studies should be focused on the introduction of conductive additive to improve the electrochemical performance of the MnO_2 materials at high scanning rate.

ACKNOWLEDGMENTS
This work was financially supported by the Natural Science Foundation of China under Grants Nos.51072131, 51202121 and 51232005, Shenzhen Projects for Basic Research, Guangdong Province Innovation R&D Team Plan for Energy and Environmental Materials (No.2009010025).

References

1. B.E. Conway., *Electrochemical Supercapacitor Scientific Fundamentals and Technological Applications*, Kluwer Academic/Plenum Press, New York, 1999.
2. J.P. Zheng, *Electrochem. Solid ST.* 2 (1999) 359-361.
3. H.Y. Lee, J.B. Goodenough, *J. Solid State Chem.* 144 (1999) 220-223.
4. C.Y. Yu, C. Chu, S.J. Chou, M.R. Chao, C.M. Yeh, D.Y. Lo, Y.C. Su, Y.M. Horng, B.C. Weng, J.G. Tsay, K.C. Huang, *Poultry Sci.* 87 (2008) 1544-1549.
5. J.B. Fei, Y. Cui, X.H. Yan, W. Qi, Y. Yang, K.W. Wang, Q. He, J.B. Li, *Adv. Mater.* 20 (2008) 452-+.
6. V. Subramanian, H.W. Zhu, R. Vajtai, P.M. Ajayan, B.Q. Wei, *J. Phys. Chem. B* 109 (2005) 20207-20214.
7. H.M. Chen, J.H. He, C.B. Zhang, H. He, *J. Phys. Chem. C* 111 (2007) 18033-18038.
8. S. Devaraj, N. Munichandraiah, *J. Electrochem. Soc.* 154 (2007) A80-A88.
9. C.J. Xu, B.H. Li, H.D. Du, F.Y. Kang, Y.Q. Zeng, *J. Power Sources* 180 (2008) 664-670.
10. B.L. Cushing, V.L. Kolesnichenko, C.J. O'Connor, *Chem. Rev.* 104 (2004) 3893-3946.
11. P.A. Winsor, *Chem.Rev* 68(1968).
12. W. Zhang, X. Qiao, J. Chen, *Mat. Sci. Eng., B* 142 (2007) 1-15.
13. K. Holmberg, *J. Colloid Interface Sci.* 274 (2004) 355-364.
14. V. Uskokovic, Drofenik, M, *Sur. Rev. and Lett.* 2 (APR 2005) 239-277.
15. M.P. Pileni, *J. Phys. Chem. C* 111 (2007) 9019-9038.
16. I. Lisiecki, *J. Phys. Chem. B* 109 (2005) 12231-12244.
17. R. Ranjan, S. Vaidya, P. Thaplyal, M. Qamar, J. Ahmed, A.K. Ganguli, *Langmuir* 25 (2009) 6469-6475.
18. A.K. Ganguli, A. Ganguly, S. Vaidya, *Chem. Soc. Rev.* 39 (2010) 474-485.
19. M.L. Curri, A. Agostiano, L. Manna, M. Della Monica, M. Catalano, L. Chiavarone, V. Spagnolo, M. Lugara, *J. Phy. Chem. B* 104 (2000) 8391-8397.
20. G. Palazzo, F. Lopez, M. Giustini, G. Colafemmina, A. Ceglie, *J. Phy. Chem. B* 107 (2003) 1924-1931.
21. J.L. Barrett EP, Halenda PP, *J. Am. Chem. Soc.* 73 (1951) 373–80.
22. S. Devaraj, N. Munichandraiah, *J. Solid State Electrochem.* 12 (2008) 207-211
23. D.Y. Zhai, B.H. Li, H.D. Du, G.Y. Gao, L. Gan, Y.B. He, Q.H. Yang, F.Y. Kang, *Carbon* 50 (2012) 5034-5043.